Letter

Proximity-induced sequence of field transitions in the Kitaev candidate $BaCo_2(AsO_4)_2$

Pavel A. Maksimov *

Bogolyubov Laboratory of Theoretical Physics, Joint Institute for Nuclear Research, Dubna, Moscow Region 141980, Russia and M. N. Miheev Institute of Metal Physics, Ural Branch of Russian Academy of Sciences, S. Kovalevskaya Street 18, 620990 Ekaterinburg, Russia

(Received 21 August 2023; accepted 30 October 2023; published 13 November 2023)

We study field-induced phase transitions of the minimal exchange model proposed earlier for $BaCo_2(AsO_4)_2$, a candidate for the Kitaev honeycomb model, using numerical minimization of classical spin clusters. We show that an experimentally observed sequence of steplike transitions in magnetic field is realized in the phase diagram of the minimal model. Surprisingly, an intermediate up-up-down plateau phase is stabilized only in the proximity of a double-zigzag–zigzag phase boundary. We systematically map out the region of stability of an experimentally observed cascade of transitions and argue that $BaCo_2(AsO_4)_2$ exchange parameters are close to a region of strong phase competition, which can explain the suppressed saturation field.

DOI: 10.1103/PhysRevB.108.L180405

Introduction. The Kitaev $S = 1/2$ honeycomb exchange model [1] is exactly solvable and has a quantum spin liquid (QSL) ground state, a correlated state without long-range magnetic order [2,3]. The model involves exchanges on three types of bonds of the honeycomb lattice with compasslike Ising interactions of three different spin axes [4] and was shown to host exotic Majorana and vison excitations. The search for materials that can host QSL is invigorated by the promise of application of its excitations in topologically protected quantum computation [1,5–7].

Honeycomb d^5 Mott insulators with strong spin-orbit coupling and edge-sharing ligand octahedra were proposed by Jackeli and Khaliullin [8] to host the Kitaev honeycomb model. Subsequent experiments on α-$RuCl_3$ [9,10] and Na_2IrO_3 [11,12], indeed, indicated the presence of Kitaev-type anisotropic exchanges, which was also supported by *ab initio* calculations [13–18]. However, the existence of additional interactions allowed by the symmetry of the lattice [19,20], as well as sizable third-neighbor exchanges, yields antiferromagnetic zigzag magnetic order in these materials. Nonetheless, the search for Kitaev interactions encouraged ongoing synthesis and analysis of new materials based on honeycomb [21–31] and triangular lattices [32–34].

$BaCo_2(AsO_4)_2$ (BCAO) was recently proposed as a platform for the Kitaev honeycomb model [35] in a new class of compounds with d^7 Co^{2+} ions, which were introduced as an alternative path towards Kitaev interactions [36–39]. In Co-based materials spin-orbit coupling yields the lowest effective doublet in the $L = 1$, $S = 3/2$ state, while additional hopping paths due to active e_g orbitals were suggested to increase Kitaev exchange [40]. This mechanism was supported by experimental evidence in various honeycomb materials [41–46], as well as triangular lattice Kitaev compounds [47].

Early neutron scattering experiments on $BaCo_2(AsO_4)_2$ indicated a spiral ground state with a $\mathbf{Q} = (0.25, 0)$ ordering vector [48], which is stabilized in the classical Heisenberg model by the competition of first- and third-neighbor interactions, J_1 and J_3. However, more refined polarized neutron-diffraction data [49] pointed to a previously undetected double-zigzag ground state, which has the same periodicity but a collinear $\uparrow\uparrow\downarrow\downarrow$ structure. It was shown later that this enigmatic state can be stabilized either by quantum fluctuations in the narrow region of the isotropic J_1-J_3 model [50], or by extension of the Heisenberg Hamiltonian by third-neighbor bond-dependent Kitaev-type coupling [51].

Generally, candidate materials for Kitaev interactions can require a large exchange parameter phase space to describe their magnetic properties, and the experimental extraction of the couplings may become highly challenging; see, as an example, the story of α-$RuCl_3$ [52]. Field-induced behavior, especially if it involves multiple phase transitions, can provide extremely useful information for the investigation of magnetic Hamiltonians [53]. In this Letter, we address peculiar experimentally observed feature of $BaCo_2(AsO_4)_2$, a field-induced sequence of phase transitions, which includes an up-up-down (UUD) $\uparrow\uparrow\downarrow$ 1/3-plateau state [35,48]. This sequence of transitions can also be seen in the magnetic spectrum of $BaCo_2(AsO_4)_2$ in terahertz measurements [54,55]. Moreover, the saturation field appears to be strongly suppressed relative to the order of exchange interactions: $g\mu_B H_s/|J_1| \simeq 0.03$. Using numerical minimization of classical spin clusters up to 144 sites, we study magnetic field phase transitions of a model proposed in Ref. [51] for $BaCo_2(AsO_4)_2$ and show that the 1/3 plateau appears in the cascade of field-induced phases only in the vicinity of the zero-field $\mathbf{Q} = (1/3, 0)$ state, which is intermediate between double-zigzag and zigzag states. Moreover, we map out a region where parameters of the model can fit experimentally observed ranges of field-induced phases, these results are summarized in Fig. 1.

*maksimov@theor.jinr.ru

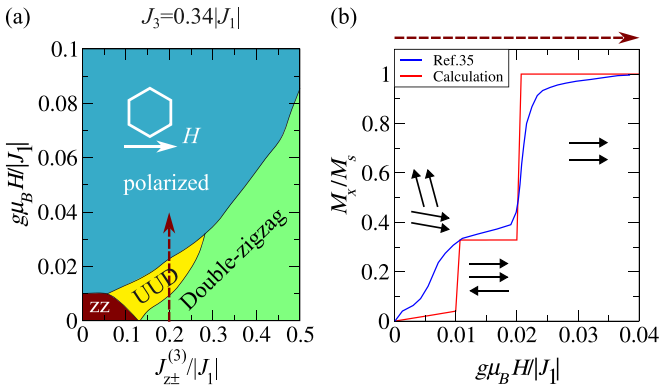

FIG. 1. A sketch of the summarized results presented in this Letter. (a) Field phase diagram of the minimal model (1) for $J_3 = 0.34|J_1|$ as a scan along $J^{(3)}_{z\pm}$, obtained with numerical minimization of classical spins. The honeycomb lattice of $BaCo_2(AsO_4)_2$ with the direction of the magnetic field used in Hamiltonian (1) is shown in the inset. (b) Magnetization along the x axis, calculated for $J^{(3)}_{z\pm} = 0.2|J_1|$ with double-zigzag, up-up-down, and polarized phases shown. Measurements from Ref. [35] are also reproduced.

The model and field phase diagram. There have been multiple attempts to establish exchanges in $BaCo_2(AsO_4)_2$ from both neutron scattering data [56] and *ab initio* calculations [51,57]. We would like to argue that the model proposed in Ref. [51] sufficiently describes both a unique zero-field ground state and the peculiar sequence of field-induced phase transitions.

The exchange Hamiltonian used in this Letter, which was coined as a "minimal" model for $BaCo_2(AsO_4)_2$ [51], is given by

$$\begin{aligned}\hat{\mathcal{H}}_{\rm min} = &-g\mu_B H\sum_i S^x_i + \sum_{\langle ij\rangle_1} J_1\left(S^x_i S^x_j + S^y_i S^y_j + \Delta_1 S^z_i S^z_j\right)\\ &+\sum_{\langle ij\rangle_3} J_3\left(S^x_i S^x_j + S^y_i S^y_j + \Delta_3 S^z_i S^z_j\right)\\ &- J^{(3)}_{z\pm}\left[\left(S^x_i S^z_j + S^z_i S^x_j\right)c_\alpha + \left(S^y_i S^z_j + S^z_i S^y_j\right)s_\alpha\right], \qquad (1)\end{aligned}$$

where $c_\alpha \equiv \cos\varphi_\alpha$ and $s_\alpha \equiv \sin\varphi_\alpha$, with the bond-dependent phases $\varphi_\alpha = \{0, 2\pi/3, -2\pi/3\}$ for the three types of first- and third-neighbor bonds $\boldsymbol{\delta}_\alpha$ and $\boldsymbol{\delta}^{(3)}_\alpha$, shown in Fig. 2(a). Note that this model is written relative to the crystallographic $\{x, y, z\}$ axes shown in Fig. 2(a), which are defined by the plane of the honeycomb lattice. In Eq. (1) we also include magnetic field parallel to x. The bond-independent terms in this Letter are assumed to be of easy-plane XY type: $\Delta_1 = \Delta_3 = 0$. The bond-dependent term $J^{(3)}_{z\pm}$ is related to exchanges of the extended Kitaev-Heisenberg model,

$$\hat{\mathcal{H}}_{\rm KH} = \sum_{\langle ij\rangle_n} \mathbf{S}^{\rm T}_i \hat{J}^{(n)}_\alpha \mathbf{S}_j,\ \hat{J}^{(n)}_{\rm X} = \begin{pmatrix} {\rm J}_n + K_n & \Gamma'_n & \Gamma'_n \\ \Gamma'_n & {\rm J}_n & \Gamma_n \\ \Gamma'_n & \Gamma_n & {\rm J}_n \end{pmatrix}, \qquad (2)$$

which is written relative to the cubic axes {x, y, z} defined by ion-ligand bonds [see Fig. 2(a)]. There are three types of bonds α = X,Y,Z, as shown in Fig. 2(a), for both $n = 1$ nearest-neighbor and $n = 3$ third-neighbor interactions. Interaction on the X bond is given in Eq. (2); the exchange

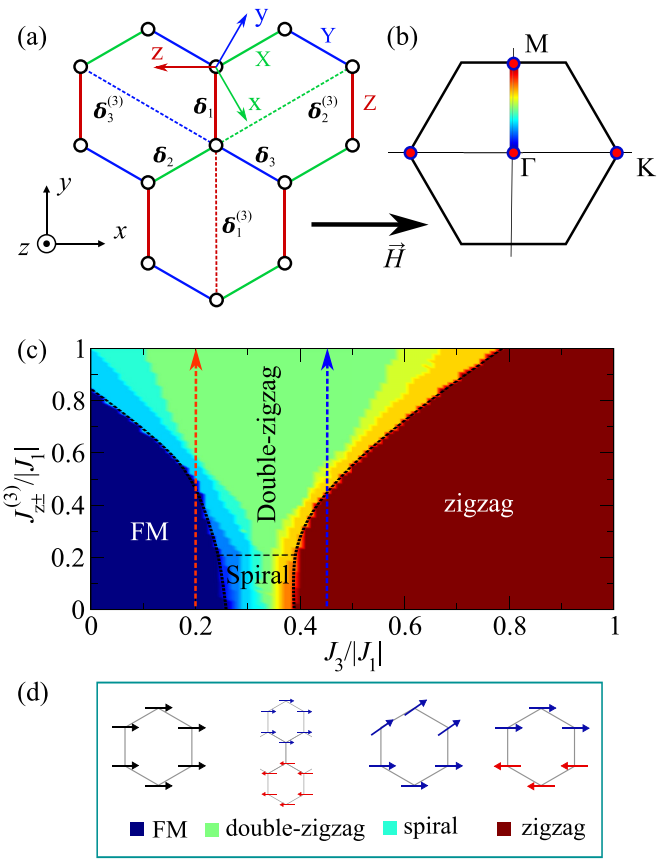

FIG. 2. (a) Honeycomb lattice with three types of nearest- and third-neighbor bonds indicated by color. The crystallographic and cubic axes, $\{x, y, z\}$ and {x, y, z}, correspond to two representations of the extended Kitaev-Heisenberg model (see text). The direction of the magnetic field is also shown. (b) Brillouin zone (BZ) of the honeycomb lattice with high-symmetry points marked. The color bar illustrates the value of the ordering vector $\mathbf{Q}$ in the phase diagram in (c). (c) Phase diagram of the model (1) in zero field, reproduced from Ref. [51]. Representative scans used in Fig. 3 are shown with dashed arrows. (d) Sketches of primary phases in the phase diagram in (c).

matrix on the Y and Z bonds is obtained through a cyclic permutation. Note that the models using the crystallographic and cubic axes are equivalent and related to each other through a linear transformation [51,58,59].

The phase diagram of the J_1-J_3-$J^{(3)}_{z\pm}$ model (1) for $J_1 < 0$ and $H = 0$ is shown in Fig. 2(c) and was calculated in Ref. [51] in classical and quantum $S = 1/2$ limits. In the classical limit, for $J^{(3)}_{z\pm} = 0$ there is a transition from a ferromagnetic (FM) to zigzag (ZZ) state via intermediate spiral states, whose ordering vectors change gradually from Γ to M [60]. The magnitude of the ordering vector of the phases in Fig. 2(c) is indicated in color, and the corresponding color bar is shown in Fig. 2(b). When $J^{(3)}_{z\pm}$ is increased, the double-zigzag state becomes stabilized in a wide region of the phase diagram both in the classical limit and for $S = 1/2$ [51]. Note that there are intermediate phases with various periodicities between FM and double zigzag, such as the $\mathbf{Q} = (1/6, 0)$ "triple zigzag," as well as the $\mathbf{Q} = (1/3, 0)$ UUD state between double-zigzag and ZZ. The structure of these states

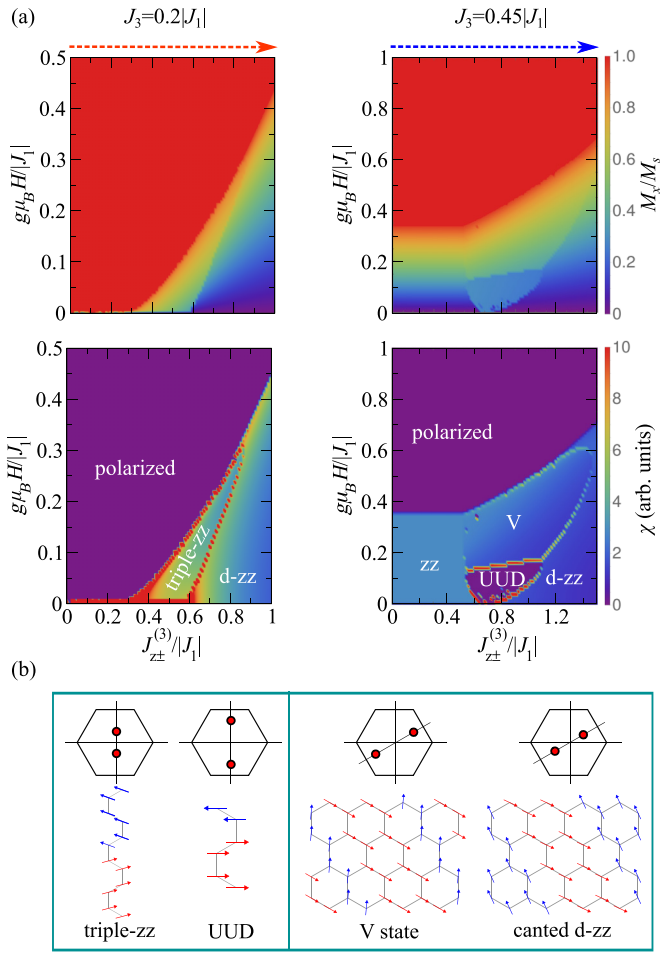

FIG. 3. (a) Intensity plots of magnetization and magnetic susceptibility for two representative values of J_3, shown as scans along $J^{(3)}_{z\pm}$, with phases indicated. (b) Sketches of the phases above with their ordering vectors shown in the BZ.

and their ordering vectors in the Brillouin zone are shown in Fig. 3(b).

In order to explore field phase transitions and how these intermediate phases affect the field behavior, we perform two calculations for representative values of third-neighbor interaction, $J_3 = 0.2|J_1|$ and $J_3 = 0.45|J_1|$ [shown with dashed arrows in Fig. 2(c)], where we plot the phase diagram in the $J^{(3)}_{z\pm}$-H axes. We perform numerical minimization of the classical energy of Hamiltonian (1) on various clusters of up to 12×12 sites using the *Mathematica* software to identify the phases, with a subsequent minimization on smaller clusters to obtain phase boundaries. The result is shown in Fig. 3(a) as an intensity plot of magnetization M_x and magnetic susceptibility $\chi = dM_x/dH$.

For $J_3 = 0.2$ and small values of $J^{(3)}_{z\pm}$ there is a direct transition from a FM to a polarized state. For $0.4 < J^{(3)}_{z\pm}/|J_1| < 0.6$ the ground state is the canted triple-zigzag state, which further gradually cants towards saturation for $H > 0$. At large $J^{(3)}_{z\pm}$, the zero-field double-zigzag state with three C_3-symmetric domains selects only two domains of the canted double-zigzag state, those closest to the field direction. This canted double-zigzag state is illustrated in Fig. 3(b). This situation is similar to the selection of zigzag domains in magnetic field in α-$RuCl_3$ [61], in which three domains are degenerate in zero field but for $H > 0$ only some are selected due to the presence of Kitaev terms [62]. Note that there is a region with an intermediate triple-zigzag state at high fields before double-zigzag reaches saturation.

For $J_3 = 0.45$ we observe even more intricate field behavior. First, for low values of $J^{(3)}_{z\pm}$, when the zero-field state is zigzag, as magnetic field is increased, there is only canting of spins in the ZZ state towards the direction of the field without phase transition, which is illustrated by the absence of singularities in the intensity plot for magnetic susceptibility χ. As $J^{(3)}_{z\pm}$ increases, the $\mathbf{Q} = (1/3, 0)$ UUD phase becomes the ground state, and it is presented as a 1/3 plateau as magnetic field is increased, until there is a transition to a canted V state at larger fields. Note that this state is analogous to the V state of the triangular lattice antiferromagnet in magnetic field [63–65]. For large enough $J^{(3)}_{z\pm}$, deep in the double-zigzag state, magnetic field induces canting of spins towards the x direction only until saturation.

The most interesting situation occurs in the vicinity of the transition between UUD and the double-zigzag state around $J^{(3)}_{z\pm} = 0.9|J_1|$, where the UUD state extends its region of stability as magnetic field increases, which results in the transition from a double-zigzag state to a UUD state, similar to what is observed in experiments on BCAO [35,48,54,55]. Notably, this transition occurs only near the zero-field phase boundary between the double-zigzag and UUD state. Therefore, the observation of this transition allows us to map out the region of parameters applicable to BCAO. However, classical analysis shows that at high field there is an intermediate V state before full polarization, which is not observed experimentally. We would like to argue that quantum fluctuations may be responsible for modifications to the field phase diagram.

Quantum effects and parameter fit. Quantum fluctuations in the case of $S = 1/2$ magnetic moments, such as the lowest doublet of BCAO, are known to strongly affect the magnetic phase diagram compared to classical calculations, with the 1/3 plateau of the triangular lattice antiferromagnet being a prime example [65]. Since quantum calculations can be demanding, it was shown that their effect can be simulated by including biquadratic coupling to the classical model, which can be derived as the first order of quantum fluctuations [66–69] or used *ad hoc* for various frustrated magnets [65,70–72].

We also explore how quantum fluctuations, approximated by biquadratic coupling

$$-B \sum_{\langle ij \rangle_1} (\mathbf{S}_i \mathbf{S}_j)^2, \tag{3}$$

affect the field phase diagram of model (1). The results for $B = 0.04|J_1|$ are shown in Fig. 4 for two representative values of J_3. This value is the lowest that can suppress V state and is of the same order as earlier estimates [67–69]. One can see that the collinear UUD state is stabilized in a wider region of parameters, while the V state is not present in the field phase diagram in Fig. 4 compared to Fig. 3, leading to an experimentally observed

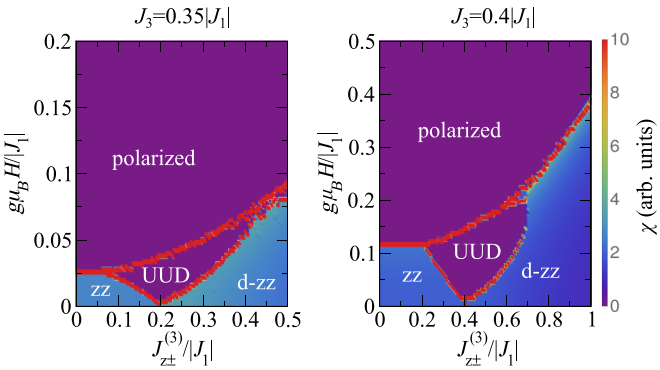

FIG. 4. Intensity plots of the magnetic susceptibility for two representative values of third-neighbor interaction $J_3 \gtrsim 0.3|J_1|$ with phases indicated for the model (1) with biquadratic coupling (3) included, $B = 0.04|J_1|$.

double-zigzag → UUD → saturation sequence in a wide region of the phase diagram.

We also checked other values of B up to $0.12|J_1|$ and confirmed very weak changes in the results with the value of biquadratic coupling. This is because zero-field and field-induced phases in the studied region of the phase diagram are nearly collinear. Therefore, biquadratic coupling is a constant and does not affect the transitions after quantum effects are taken into account. Thus, in this Letter we present only results for $B = 0.04|J_1|$.

Moreover, we can map out the region of the J_3-$J^{(3)}_{z\pm}$ phase diagram, where the values of critical magnetic fields fit experimental measurements, H_{c1} and H_{c2}. Here, H_{c1} is the critical field of the double-zigzag → UUD transition, and H_{c2} is the saturation field. According to magnetization measurements [35,48], $H_{c1} = 0.26T$, and $H_{c2} = 0.52T$. We break the parameter fit procedure into two steps. First, we plot H_{c1}/H_{c2} as an intensity plot in the $J_3 - J^{(3)}_{z\pm}$ phase diagram in Fig. 5(a), where we can see that such a sequence of field-induced transitions occurs only in the proximity of the UUD state. When H_{c1}/H_{c2} reaches 1 in the phase diagram in Fig. 5(a), it implies

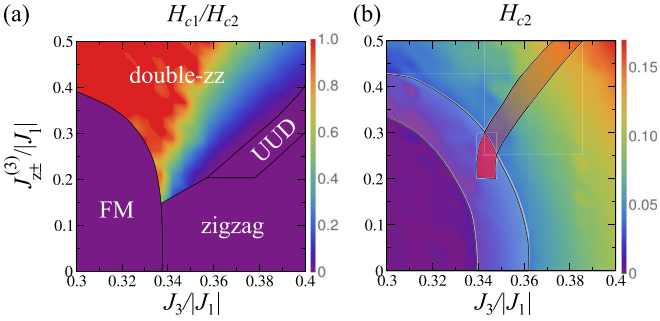

FIG. 5. (a) Intensity plot of H_{c1}/H_{c2}, two critical fields of the double-zigzag → UUD → saturated sequence of transitions. When $H_{c1}/H_{c2} = 1$, there is only a direct transition from the canted double-zigzag to the polarized state. (b) Intensity plot of saturation field H_{c2} in units of $g\mu_B H/|J_1|$. The blue shaded region indicates parameters with $0.02 < g\mu_B H_{c2}/|J_1| < 0.04$. The red shaded region marks parameters with $0.4 < H_{c1}/H_{c2} < 0.6$. The intersection of these regions gives optimal parameter sets that fit experimentally observed values.

the absence of intermediate UUD state and a direct transition from the canted double-zigzag to a polarized state. The range of parameters where $0.4 < H_{c1}/H_{c2} < 0.6$ is shown by the red shaded region in Fig. 5(b), fitting the experimentally observed ratio of 0.5.

Next, we use $g = 5.2$ [35] to map the region of the phase diagram with saturation field $H_{c2} = 0.52T$. Various experimental estimates of nearest-neighbor coupling range from $J_1 = -3.3$ meV [73] to $J_1 = -7.6$ meV [56] (see also Refs. [51,57] for *ab initio* calculations with similar results), which yields an allowed region of values of $g\mu_B H_{c2}/|J_1|$ of 0.02–0.04. The parameters of Hamiltonian (1) which produce this range of critical fields are shown by the blue shaded region in Fig. 5(b). Combining the range of critical fields with the requirement for the ratio H_{c1}/H_{c2}, we obtain the region for the exchange parameters for $BaCo_2(AsO_4)_2$ that fit field-induced transitions observed in experiment, shown as the intersection of two shaded regions. We also performed these calculations for the XXZ anisotropy $\Delta_1 = \Delta_3 = 0.4$, which was motivated by a spin-wave theory fit to the field behavior of the $\mathbf{k} = 0$ mode of $BaCo_2(AsO_4)_2$ in the polarized phase [56]. The region of optimal parameters for $\Delta = 0.4$ is very similar to the results in Fig. 5(b) due to the coplanar nature of the states in the phase diagram, which makes classical energies of the zero-field and field-induced states independent of the choice of Δ.

In order to illustrate the goodness of the fit, we plot magnetization for a representative set of parameters $J^{(3)}_{z\pm} = 0.2|J_1|$ and $J_3 = 0.34|J_1|$ in Fig. 1(b) together with experimental values from Ref. [35] (we use $J_1 = -7.6$ meV). There is a degree of discrepancy, which can be attributed to the broadening of transitions due to the finite temperature, whereas our calculations are performed at zero temperature. However, we can still see that our calculations provide a very good fit for the experimental magnetization. Notably, the experimentally observed saturation field is rather small, and we see from Fig. 5(b) that the reason for that is the proximity of the optimal parameter region to the region with multiple phases in competition. Note that compared to previous estimates of exchanges in BCAO [51], this parameter set requires larger Γ_1 and Γ'_1 due to the stronger easy-plane anisotropy, as well as larger K_3, Γ_3, and Γ'_3 to describe the presence of non-negligible $J^{(3)}_{z\pm}$.

Moreover, in order to check that a rather large bond-dependent term $J^{(3)}_{z\pm}$, which is necessary for the explanation of the features studied in this Letter, does not introduce anomalies to the magnetic spectrum, we performed linear spin-wave calculations for $J^{(3)}_{z\pm} = 0.4|J_1|$, $J_3 = 0.34|J_1|$, and $J_1 = -7.6$ meV. The result is shown in Fig. 6, with energy in units of meV for a direct comparison with inelastic neutron scattering data [56,74]. While we cannot expect complete agreement with experimental data, we see that our calculation does reproduce multiple features of the spectrum. For instance, there are low-energy modes with a small gap around 1 meV (1.5 meV experimentally), as well as high-energy modes around 11 and 13 meV, in agreement with a 12 meV mode in the neutron scattering data [74]. Moreover, there is a rather flat mode around 3.5 meV in Fig. 6 which was also observed in the neutron scattering data [56]. Note that even in the presence of large $J^{(3)}_{z\pm} = 3$ meV, the gap is rather small, which means that the model proposed in this Letter

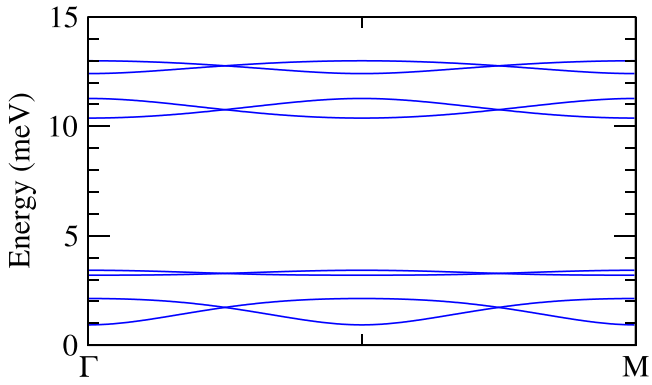

FIG. 6. Spin-wave magnetic spectrum in the double-zigzag state for $J_1 = -7.6$ meV, $J_{z\pm}^{(3)} = 0.4|J_1|$, and $J_3 = 0.34|J_1|$.

is physically viable. Nonetheless, we should note that the spin-wave energies in Fig. 6 do not agree precisely with neutron scattering data and a careful fitting of the magnetic spectrum presumably requires all eight parameters of the extended Kitaev-Heisenberg model, placing such a fit beyond the scope of this work.

Discussion. Establishing the parameters of a model with multiple allowed exchange parameters, like the extended Kitaev-Heisenberg model, can be cumbersome in a lot of cases. Experiments in the magnetic field, which can include several transitions, may strongly assist with setting boundaries on exchanges. We performed an analysis of the field-induced phases of the anisotropic exchange model suggested previously for $BaCo_2(AsO_4)_2$ using numerical minimization of classical spins, and we observed a plethora of phase transitions in various parts of the zero-field phase diagram. We showed that an experimentally established double-zigzag → UUD → saturated phase sequence is stabilized by quantum fluctuations only in the proximity of the double-zigzag phase boundary. By scanning through the phase space, we fit critical fields to the experimentally observed values and narrowed down the parameters which provide the best agreement. As it turns out, the presence of third-neighbor bond-dependent exchange $J_{z\pm}^{(3)}$ is necessary, and in our analysis we were able to put limits on its values. We should note that previous attempts at calculating exchanges for $BaCo_2(AsO_4)_2$ are not in precise agreement with each other. However, they all point to an easy-plane XXZ J_1-J_3 model, with the ratio of nearest- and third-neighbor exchanges being around 0.3, and the presence of small, but non-negligible, bond-dependent corrections [51,56,57,73]. Our parameter set supports this notion and further promotes the idea that a third-neighbor bond-dependent term is crucial for the physics of $BaCo_2(AsO_4)_2$. Moreover, recent measurements on a related compound $BaCo_2(PO_4)_2$ indicated a very similar field-induced behavior [75], making our results applicable to a broad class of materials.

Acknowledgments. I would like to thank S. Streltsov and S. Chernyshev for useful discussions. I acknowledge support from the Russian Science Foundation via Project No. 23-12-00159.

[1] A. Kitaev, Anyons in an exactly solved model and beyond, Ann. Phys. (NY) **321**, 2 (2006).
[2] L. Balents, Spin liquids in frustrated magnets, Nature (London) **464**, 199 (2010).
[3] L. Savary and L. Balents, Quantum spin liquids: A review, Rep. Prog. Phys. **80**, 016502 (2017).
[4] Z. Nussinov and J. van den Brink, Compass models: Theory and physical motivations, Rev. Mod. Phys. **87**, 1 (2015).
[5] S. B. Bravyi and A. Y. Kitaev, Quantum codes on a lattice with boundary, arXiv:quant-ph/9811052.
[6] A. Y. Kitaev, Fault-tolerant quantum computation by anyons, Ann. Phys. (NY) **303**, 2 (2003).
[7] C. Nayak, S. H. Simon, A. Stern, M. Freedman, and S. Das Sarma, Non-Abelian anyons and topological quantum computation, Rev. Mod. Phys. **80**, 1083 (2008).
[8] G. Jackeli and G. Khaliullin, Mott insulators in the strong spin-orbit coupling limit: From Heisenberg to a quantum compass and Kitaev models, Phys. Rev. Lett. **102**, 017205 (2009).
[9] K. W. Plumb, J. P. Clancy, L. J. Sandilands, V. V. Shankar, Y. F. Hu, K. S. Burch, H.-Y. Kee, and Y.-J. Kim, α-$RuCl_3$: A spin-orbit assisted Mott insulator on a honeycomb lattice, Phys. Rev. B **90**, 041112(R) (2014).
[10] A. Banerjee, C. A. Bridges, J. Q. Yan, A. A. Aczel, L. Li, M. B. Stone, G. E. Granroth, M. D. Lumsden, Y. Yiu, J. Knolle, S. Bhattacharjee, D. L. Kovrizhin, R. Moessner, D. A. Tennant, D. G. Mandrus, and S. E. Nagler, Proximate Kitaev quantum spin liquid behaviour in a honeycomb magnet, Nat. Mater. **15**, 733 (2016).
[11] Y. Singh, S. Manni, J. Reuther, T. Berlijn, R. Thomale, W. Ku, S. Trebst, and P. Gegenwart, Relevance of the Heisenberg-Kitaev model for the honeycomb lattice iridates A_2IrO_3, Phys. Rev. Lett. **108**, 127203 (2012).
[12] S. K. Choi, R. Coldea, A. N. Kolmogorov, T. Lancaster, I. I. Mazin, S. J. Blundell, P. G. Radaelli, Y. Singh, P. Gegenwart, K. R. Choi, S.-W. Cheong, P. J. Baker, C. Stock, and J. Taylor, Spin waves and revised crystal structure of honeycomb iridate Na_2IrO_3, Phys. Rev. Lett. **108**, 127204 (2012).
[13] V. M. Katukuri, S. Nishimoto, V. Yushankhai, A. Stoyanova, H. Kandpal, S. Choi, R. Coldea, I. Rousochatzakis, L. Hozoi, and J. van den Brink, Kitaev interactions between j = 1/2 moments in honeycomb Na_2IrO_3 are large and ferromagnetic: Insights from *ab initio* quantum chemistry calculations, New J. Phys. **16**, 013056 (2014).
[14] Y. Sizyuk, C. Price, P. Wölfle, and N. B. Perkins, Importance of anisotropic exchange interactions in honeycomb iridates: Minimal model for zigzag antiferromagnetic order in Na_2IrO_3, Phys. Rev. B **90**, 155126 (2014).
[15] S. M. Winter, Y. Li, H. O. Jeschke, and R. Valentí, Challenges in design of Kitaev materials: Magnetic interactions from competing energy scales, Phys. Rev. B **93**, 214431 (2016).

[16] R. Yadav, N. A. Bogdanov, V. M. Katukuri, S. Nishimoto, J. van den Brink, and L. Hozoi, Kitaev exchange and field-induced quantum spin-liquid states in honeycomb α-$RuCl_3$, Sci. Rep. **6**, 37925 (2016).

[17] Y. S. Hou, H. J. Xiang, and X. G. Gong, Unveiling magnetic interactions of ruthenium trichloride via constraining direction of orbital moments: Potential routes to realize a quantum spin liquid, Phys. Rev. B **96**, 054410 (2017).

[18] C. Eichstaedt, Y. Zhang, P. Laurell, S. Okamoto, A. G. Eguiluz, and T. Berlijn, Deriving models for the Kitaev spin-liquid candidate material α-$RuCl_3$ from first principles, Phys. Rev. B **100**, 075110 (2019).

[19] J. Chaloupka, G. Jackeli, and G. Khaliullin, Zigzag magnetic order in the iridium oxide Na_2IrO_3, Phys. Rev. Lett. **110**, 097204 (2013).

[20] J. G. Rau, E. K.-H. Lee, and H.-Y. Kee, Generic spin model for the honeycomb iridates beyond the Kitaev limit, Phys. Rev. Lett. **112**, 077204 (2014).

[21] D. Ni, X. Gui, K. M. Powderly, and R. J. Cava, Honeycomb-structure RuI_3, a new quantum material related to α-$RuCl_3$, Adv. Mater. **34**, 2106831 (2022).

[22] Y. Imai, K. Nawa, Y. Shimizu, W. Yamada, H. Fujihara, T. Aoyama, R. Takahashi, D. Okuyama, T. Ohashi, M. Hagihala, S. Torii, D. Morikawa, M. Terauchi, T. Kawamata, M. Kato, H. Gotou, M. Itoh, T. J. Sato, and K. Ohgushi, Zigzag magnetic order in the Kitaev spin-liquid candidate material $RuBr_3$ with a honeycomb lattice, Phys. Rev. B **105**, L041112 (2022).

[23] H.-S. Kim, Spin-orbit-entangled nature of magnetic moments and Kitaev magnetism in layered halides, Appl. Sci. Converg. Technol. **30**, 191 (2021).

[24] D. A. S. Kaib, K. Riedl, A. Razpopov, Y. Li, S. Backes, I. I. Mazin, and R. Valentí, Electronic and magnetic properties of the RuX_3 (X = Cl, Br, I) family: Two siblings—and a cousin? npj Quantum Mater. **7**, 75 (2022).

[25] M. Abramchuk, C. Ozsoy-Keskinbora, J. W. Krizan, K. R. Metz, D. C. Bell, and F. Tafti, Cu_2IrO_3: A new magnetically frustrated honeycomb iridate, J. Am. Chem. Soc. **139**, 15371 (2017).

[26] K. Kitagawa, T. Takayama, Y. Matsumoto, A. Kato, R. Takano, Y. Kishimoto, S. Bette, R. Dinnebier, G. Jackeli, and H. Takagi, A spin–orbital-entangled quantum liquid on a honeycomb lattice, Nature (London) **554**, 341 (2018).

[27] S. M. Winter, A. A. Tsirlin, M. Daghofer, J. van den Brink, Y. Singh, P. Gegenwart, and R. Valentí, Models and materials for generalized Kitaev magnetism, J. Phys.: Condens. Matter **29**, 493002 (2017).

[28] H. Takagi, T. Takayama, G. Jackeli, G. Khaliullin, and S. E. Nagler, Concept and realization of Kitaev quantum spin liquids, Nat. Rev. Phys. **1**, 264 (2019).

[29] Y. Motome, R. Sano, S. Jang, Y. Sugita, and Y. Kato, Materials design of Kitaev spin liquids beyond the Jackeli-Khaliullin mechanism, J. Phys.: Condens. Matter **32**, 404001 (2020).

[30] A. A. Tsirlin and P. Gegenwart, Kitaev magnetism through the prism of lithium iridate, Phys. Status Solidi B **259**, 2100146 (2022).

[31] S. Trebst and C. Hickey, Kitaev materials, Phys. Rep. **950**, 1 (2022).

[32] M. Becker, M. Hermanns, B. Bauer, M. Garst, and S. Trebst, Spin-orbit physics of $j = \frac{1}{2}$ Mott insulators on the triangular lattice, Phys. Rev. B **91**, 155135 (2015).

[33] Y. Li, H. Liao, Z. Zhang, S. Li, F. Jin, L. Ling, L. Zhang, Y. Zou, L. Pi, Z. Yang, J. Wang, Z. Wu, and Q. Zhang, Gapless quantum spin liquid ground state in the two-dimensional spin-1/2 triangular antiferromagnet $YbMgGaO_4$, Sci. Rep. **5**, 16419 (2015).

[34] I. Rousochatzakis, U. K. Rössler, J. van den Brink, and M. Daghofer, Kitaev anisotropy induces mesoscopic $\mathbb{Z}_2$ vortex crystals in frustrated hexagonal antiferromagnets, Phys. Rev. B **93**, 104417 (2016).

[35] R. Zhong, T. Gao, N. P. Ong, and R. J. Cava, Weak-field induced nonmagnetic state in a Co-based honeycomb, Sci. Adv. **6**, eaay6953 (2020).

[36] R. Sano, Y. Kato, and Y. Motome, Kitaev-Heisenberg Hamiltonian for high-spin d^7 Mott insulators, Phys. Rev. B **97**, 014408 (2018).

[37] H. Liu and G. Khaliullin, Pseudospin exchange interactions in d^7 cobalt compounds: Possible realization of the Kitaev model, Phys. Rev. B **97**, 014407 (2018).

[38] S. M. Winter, Magnetic couplings in edge-sharing high-spin d^7 compounds, J. Phys. Mater. **5**, 045003 (2022).

[39] X. Liu and H.-Y. Kee, Non-Kitaev versus Kitaev honeycomb cobaltates, Phys. Rev. B **107**, 054420 (2023).

[40] H. Liu, J. Chaloupka, and G. Khaliullin, Kitaev spin liquid in *3d* transition metal compounds, Phys. Rev. Lett. **125**, 047201 (2020).

[41] H. Liu, Towards Kitaev spin liquid in *3d* transition metal compounds, Int. J. Mod. Phys. B **35**, 2130006 (2021).

[42] M. Elliot, P. A. McClarty, D. Prabhakaran, R. D. Johnson, H. C. Walker, P. Manuel, and R. Coldea, Order-by-disorder from bond-dependent exchange and intensity signature of nodal quasiparticles in a honeycomb cobaltate, Nat. Commun. **12**, 3936 (2021).

[43] L. Viciu, Q. Huang, E. Morosan, H. Zandbergen, N. Greenbaum, T. McQueen, and R. Cava, Structure and basic magnetic properties of the honeycomb lattice compounds $Na_2Co_2TeO_6$ and $Na_3Co_2SbO_6$, J. Solid State Chem. **180**, 1060 (2007).

[44] H. K. Vivanco, B. A. Trump, C. M. Brown, and T. M. McQueen, Competing antiferromagnetic-ferromagnetic states in a d^7 Kitaev honeycomb magnet, Phys. Rev. B **102**, 224411 (2020).

[45] M. Songvilay, J. Robert, S. Petit, J. A. Rodriguez-Rivera, W. D. Ratcliff, F. Damay, V. Balédent, M. Jiménez-Ruiz, P. Lejay, E. Pachoud, A. Hadj-Azzem, V. Simonet, and C. Stock, Kitaev interactions in the Co honeycomb antiferromagnets $Na_3Co_2SbO_6$ and $Na_2Co_2TeO_6$, Phys. Rev. B **102**, 224429 (2020).

[46] C. Kim, J. Jeong, G. Lin, P. Park, T. Masuda, S. Asai, S. Itoh, H.-S. Kim, H. Zhou, J. Ma, and J.-G. Park, Antiferromagnetic Kitaev interaction in $J_{\text{eff}} = 1/2$ cobalt honeycomb materials $Na_3Co_2SbO_6$ and $Na_2Co_2TeO_6$, J. Phys.: Condens. Matter **34**, 045802 (2022).

[47] C. Kim, S. Kim, P. Park, T. Kim, J. Jeong, S. Ohira-Kawamura, N. Murai, K. Nakajima, A. L. Chernyshev, M. Mourigal, S.-J. Kim, and J.-G. Park, Bond-dependent anisotropy and magnon decay in cobalt-based Kitaev triangular antiferromagnet, Nat. Phys. (2023).

[48] L. Regnault, P. Burlet, and J. Rossat-Mignod, Magnetic ordering in a planar X - Y model: $BaCo_2(AsO_4)_2$, Physica B+C (Amsterdam) **86–88**, 660 (1977).

[49] L.-P. Regnault, C. Boullier, and J. E. Lorenzo, Polarized-neutron investigation of magnetic ordering and spin dynamics in $BaCo_2(AsO_4)_2$ frustrated honeycomb-lattice magnet, Heliyon **4**, e00507 (2018).

[50] S. Jiang, S. R. White, and A. L. Chernyshev, Quantum phases in the honeycomb-lattice J_1–J_3 ferro-antiferromagnetic model, arXiv:2304.06062.

[51] P. A. Maksimov, A. V. Ushakov, Z. V. Pchelkina, Y. Li, S. M. Winter, and S. V. Streltsov, *Ab initio* guided minimal model for the "Kitaev" material $BaCo_2(AsO_4)_2$: Importance of direct hopping, third-neighbor exchange, and quantum fluctuations, Phys. Rev. B **106**, 165131 (2022).

[52] P. A. Maksimov and A. L. Chernyshev, Rethinking α-$RuCl_3$, Phys. Rev. Res. **2**, 033011 (2020).

[53] W. Steinhardt, P. A. Maksimov, S. Dissanayake, Z. Shi, N. P. Butch, D. Graf, A. Podlesnyak, Y. Liu, Y. Zhao, G. Xu, J. W. Lynn, C. Marjerrison, A. L. Chernyshev, and S. Haravifard, Phase diagram of $YbZnGaO_4$ in applied magnetic field, npj Quantum Mater. **6**, 78 (2021).

[54] X. Zhang, Y. Xu, T. Halloran, R. Zhong, C. Broholm, R. J. Cava, N. Drichko, and N. P. Armitage, A magnetic continuum in the cobalt-based honeycomb magnet $BaCo_2(AsO_4)_2$, Nat. Mater. **22**, 58 (2023).

[55] L. Y. Shi, X. M. Wang, R. D. Zhong, Z. X. Wang, T. C. Hu, S. J. Zhang, Q. M. Liu, T. Dong, F. Wang, and N. L. Wang, Magnetic excitations of the field-induced states in $BaCo_2(AsO_4)_2$ probed by time-domain terahertz spectroscopy, Phys. Rev. B **104**, 144408 (2021).

[56] T. Halloran, F. Desrochers, E. Z. Zhang, T. Chen, L. E. Chern, Z. Xu, B. Winn, M. Graves-Brook, M. B. Stone, A. I. Kolesnikov, Y. Qiu, R. Zhong, R. Cava, Y. B. Kim, and C. Broholm, Geometrical frustration versus Kitaev interactions in $BaCo_2(AsO_4)_2$, Proc. Natl. Acad. Sci. USA **120**, e2215509119 (2023).

[57] S. Das, S. Voleti, T. Saha-Dasgupta, and A. Paramekanti, XY magnetism, Kitaev exchange, and long-range frustration in the $J_{\rm eff} = \frac{1}{2}$ honeycomb cobaltates, Phys. Rev. B **104**, 134425 (2021).

[58] J. G. Rau and H.-Y. Kee, Trigonal distortion in the honeycomb iridates: Proximity of zigzag and spiral phases in Na_2IrO_3, arXiv:1408.4811.

[59] J. Chaloupka and G. Khaliullin, Hidden symmetries of the extended Kitaev-Heisenberg model: Implications for the honeycomb-lattice iridates A_2IrO_3, Phys. Rev. B **92**, 024413 (2015).

[60] E. Rastelli, A. Tassi, and L. Reatto, Non-simple magnetic order for simple Hamiltonians, Physica B+C (Amsterdam) **97**, 1 (1979).

[61] A. Banerjee, P. Lampen-Kelley, J. Knolle, C. Balz, A. A. Aczel, B. Winn, Y. Liu, D. Pajerowski, J. Yan, C. A. Bridges, A. T. Savici, B. C. Chakoumakos, M. D. Lumsden, D. A. Tennant, R. Moessner, D. G. Mandrus, and S. E. Nagler, Excitations in the field-induced quantum spin liquid state of α-$RuCl_3$, npj Quantum Mater. **3**, 8 (2018).

[62] J. A. Sears, Y. Zhao, Z. Xu, J. W. Lynn, and Y.-J. Kim, Phase diagram of α-$RuCl_3$ in an in-plane magnetic field, Phys. Rev. B **95**, 180411(R) (2017).

[63] H. Kawamura, Spin-wave analysis of the antiferromagnetic plane rotator model on the triangular lattice-symmetry breaking in a magnetic field, J. Phys. Soc. Jpn. **53**, 2452 (1984).

[64] S. E. Korshunov, Phase diagram of the antiferromagnetic XY model with a triangular lattice in an external magnetic field, J. Phys. C **19**, 5927 (1986).

[65] A. V. Chubukov and D. I. Golosov, Quantum theory of an antiferromagnet on a triangular lattice in a magnetic field, J. Phys.: Condens. Matter **3**, 69 (1991).

[66] C. L. Henley, Effective Hamiltonians and dilution effects in kagome and related anti-ferromagnets, Can. J. Phys. **79**, 1307 (2001).

[67] C. Griset, S. Head, J. Alicea, and O. A. Starykh, Deformed triangular lattice antiferromagnets in a magnetic field: Role of spatial anisotropy and Dzyaloshinskii-Moriya interactions, Phys. Rev. B **84**, 245108 (2011).

[68] G. Koutroulakis, T. Zhou, Y. Kamiya, J. D. Thompson, H. D. Zhou, C. D. Batista, and S. E. Brown, Quantum phase diagram of the $s = \frac{1}{2}$ triangular-lattice antiferromagnet $Ba_3CoSb_2O_9$, Phys. Rev. B **91**, 024410 (2015).

[69] M. E. Zhitomirsky, Real-space perturbation theory for frustrated magnets: Application to magnetization plateaus, J. Phys.: Conf. Ser. **592**, 012110 (2015).

[70] K. Penc, N. Shannon, and H. Shiba, Half-magnetization plateau stabilized by structural distortion in the antiferromagnetic Heisenberg model on a pyrochlore lattice, Phys. Rev. Lett. **93**, 197203 (2004).

[71] T. A. Kaplan, Frustrated classical Heisenberg model in one dimension with nearest-neighbor biquadratic exchange: Exact solution for the ground-state phase diagram, Phys. Rev. B **80**, 012407 (2009).

[72] A. I. Smirnov, T. A. Soldatov, O. A. Petrenko, A. Takata, T. Kida, M. Hagiwara, A. Y. Shapiro, and M. E. Zhitomirsky, Order by quenched disorder in the model triangular antiferromagnet $RbFe(MoO_4)_2$, Phys. Rev. Lett. **119**, 047204 (2017).

[73] L. Regnault, J. Boucher, J. Rossat-Mignod, J. Bouillot, R. Pynn, J. Henry, and J. Renard, Nonlinear excitations in lD and 2D magnetic systems, Physica B+C (Amsterdam) **136**, 329 (1986).

[74] L. Regnault and J. Rossat-Mignod, Phase transitions in quasi two-dimensional planar magnets, in *Magnetic Properties of Layered Transition Metal Compounds* (Springer, Dordrecht, 1990), pp. 271–321.

[75] X. Wang, R. Sharma, P. Becker, L. Bohatý, and T. Lorenz, Single-crystal study of the honeycomb XXZ magnet $BaCo_2(PO_4)_2$ in magnetic fields, Phys. Rev. Mater. **7**, 024402 (2023).